Quantification of NAD+ in human brain with 1H MR spectroscopy at 3 T: Comparison of three localization techniques with different handling of water magnetization

Martyna Dziadosz[1,2,3] | **Maike Hoefemann**[1,2,3] | **André Döring**[4] |

Malgorzata Marjańska[5] | **Edward John Auerbach**[5] | **Roland Kreis**[1,3]

[1]MR Methodology, Department for Diagnostic and Interventional Neuroradiology & Department for Biomedical Research, University of Bern, Bern, Switzerland

[2]Graduate School for Cellular and Biomedical Sciences, University of Bern, Bern, Switzerland

[3]Translational Imaging Center (TIC), Swiss Institute for Translational and Entrepreneurial Medicine, Bern, Switzerland

[4]Cardiff University Brain Research Imaging Centre (CUBRIC), School of Psychology, Cardiff University, Cardiff, UK

[5]Department of Radiology, Center for Magnetic Resonance Research, University of Minnesota, Minneapolis, Minnesota USA

Correspondence
Roland Kreis, MR Methodology, University Bern, Freiburgstr. 3, CH-3010 Bern, Switzerland.
Email: roland.kreis@insel.ch

Purpose: The detection of nicotinamide-adenine-dinucleotide (NAD+) is challenging using standard 1H MR spectroscopy, because it is of low concentration and affected by polarization-exchange with water. Therefore, this study compares three techniques to access NAD+ quantification at 3 T–one with and two without water presaturation.

Methods: A large brain volume in 10 healthy subjects was investigated with three techniques: semi-LASER with water-saturation (WS) (TE = 35 ms), semi-LASER with metabolite-cycling (MC) (TE = 35 ms), and the non-water-excitation (nWE) technique 2D ISIS-localization with chemical-shift-selective excitation (2D I-CSE) (TE = 10.2 ms). Spectra were quantified with optimized modeling in FiTAID.

Results: NAD+ could be well quantified in cohort-average spectra with all techniques. Obtained apparent NAD+ tissue contents are all lower than expected from literature confirming restricted visibility by 1H MRS. The estimated value from WS-MRS (58 μM) was considerably lower than those obtained with non-WS techniques (146 μM for MC-semi-LASER and 125 μM for 2D I-CSE). The nWE technique with shortest TE gave largest NAD+ signals but suffered from overlap with large amide signals. MC-semi-LASER yielded best estimation precision as reflected in relative Cramer-Rao bounds (14%, 21 μM/146 μM) and also best robustness as judged by the coefficient-of-variance over the cohort (11%, 10 μM/146 μM). The MR-visibility turned out as 16% with WS and 41% with MC.

Conclusion: Three methods to assess NAD+ in human brain at 3 T have been compared. NAD+ could be detected with a visibility of ∼41% for the MC method. This may open a new window for the observation of pathological changes in the clinical research setting.

KEYWORDS
brain, detectability, fitting, magnetization exchange, modeling, MR spectroscopy, NAD+, precision, quantification, saturation transfer

1 | INTRODUCTION

Nicotinamide-adenine-dinucleotide in its oxidized (NAD$^+$) and reduced (NADH) forms plays an important role in the regulation of metabolism. Recent studies suggested that it is not only essential in energy metabolism and mitochondrial functions, but also in calcium homeostasis, gene expression, or cell aging and death, connecting it to a plethora of brain diseases and making it a metabolite of high interest for clinical studies.[1,2] However, in vivo detection of NAD$^+$ and NADH is challenging.

^{31}P MR spectroscopy (MRS) has been used to measure the total pool of NAD$^+$ and NADH. Moving to higher fields allowed separate detection of the overlapping NAD$^+$ and NADH signals in animals and humans.[3,4] With ^{1}H MRS, the detection of NAD$^+$ proved to be difficult, not only due to its low concentration, but mainly because of saturation transfer from water,[5] where the water signal in standard ^{1}H-MRS is suppressed by repeated saturation pulses preceding the acquisition of the metabolite signals. Thus, indirect polarization exchange between NAD$^+$ and water leads to strong attenuation of the NAD$^+$ signal. In particular, it was shown in vitro that addition of alcohol dehydrogenase, which binds NAD$^+$, results in strong signal attenuation that is not seen for pure aqueous solutions of NAD$^+$.[6] Frequency-selective excitation of the metabolite resonances without affecting the water magnetization (using so-called non-water-excitation [nWE] sequences[7,8]) was proposed to overcome this issue and to make in vivo detection of NAD$^+$ possible in human brain, in particular at 7T.[6,9] However, this comes at the cost of limited availability and possibly lower robustness. Hence, an evaluation at 3 T with different techniques seems warranted.

For NAD$^+$, the targeted resonances are in the downfield region, in particular >8.5 ppm, where no other signals are detectable with standard MRS at medium TEs (>25 ms). At lower fields, it may, however, still be challenging to quantify NAD$^+$ in this downfield region with nWE methods because of signal overlap with large unknown amide signals in the spectral range of 8 to 8.5 ppm, which become prominent with nWE techniques[10] and provide a large baseline signal >8.5 ppm at 3 T where the relative resolution is lower than at very high fields. The reduced form of NAD, NADH, does unfortunately not feature isolated peaks in the downfield region,[5] and with its even lower concentration remained undetectable by ^{1}H MRS even at very high fields.[5]

The extent of signal attenuation for NAD$^+$ in standard in vivo MRS measurements with water suppression (WS) has not been quantified hitherto. Thus, with a suitable experimental setup, it might be possible to detect the remaining NAD$^+$ signal with clinically useful precision even at 3 T and standard MRS sequences. One possibility to improve the detectability of low-concentration metabolites in general is to aim at an optimal SNR with good spectral resolution. This can be achieved by using a high number of averages and by choosing a large volume of interest (VOI). In a previous study,[11] the optimal VOI size for a comparable experimental setting using a semi-LASER sequence[12,13] with optimized acquisition parameters was found to be around 75 cm^3 at 3 T, where fitting uncertainties reflected in the Cramér-Rao lower bounds (CRLB) were found to be minimal.

In this study, we present a comparison of three methods to access NAD$^+$ quantification on a clinical 3T scanner: (1) standard semi-LASER[12,13] with VAPOR WS; (2) semi-LASER with metabolite-cycling (MC),[14,15] that is, a technique that avoids water presaturation, but includes water excitation (and thus saturation for the subsequent acquisition) in the localization module; (3) 2D ISIS-localization with chemical-shift-selective excitation (2D I-CSE),[10] that is, a nWE technique.

Visibility as well as precision and robustness of quantification of the NAD$^+$ signal recorded with these techniques were targeted as reflected in the estimated tissue content, the CRLB and the SD of the content estimates over a cohort of 10 healthy subjects.

2 | METHODS

2.1 | Data acquisition

In vivo data were acquired from 12 healthy subjects (8 male, 4 female; 36 ± 11 years of age) on a 3T MR scanner (Prisma, Siemens, Erlangen, Germany) using a 64-channel receive-only head coil (44 channels used, excluding coil-elements in the neck region). Spectra were acquired with a spectral width of 4000 Hz and 4096 data points. A VOI size of $50 \times 75 \times 20$ mm^3 = 75 cm^3 was chosen according to the optimum found in Ref. [11] The VOI was placed superior to the lateral ventricles (Figure 1A, ~5 mm spacing to the roof of the ventricles).

The manufacturer's second-order shimming routine (option "brain" with a higher resolution for the field map than in the default mode) was used. Measurements were split into two sessions for the three sequences (WS-semi-LASER, MC-semi-LASER, and 2D I-CSE). In a first measurement block, 10 subjects were examined using WS-semi-LASER. A year later, the two nWS techniques were evaluated in 10 subjects (8 from the first cohort and 2 replacements with matching age and sex).

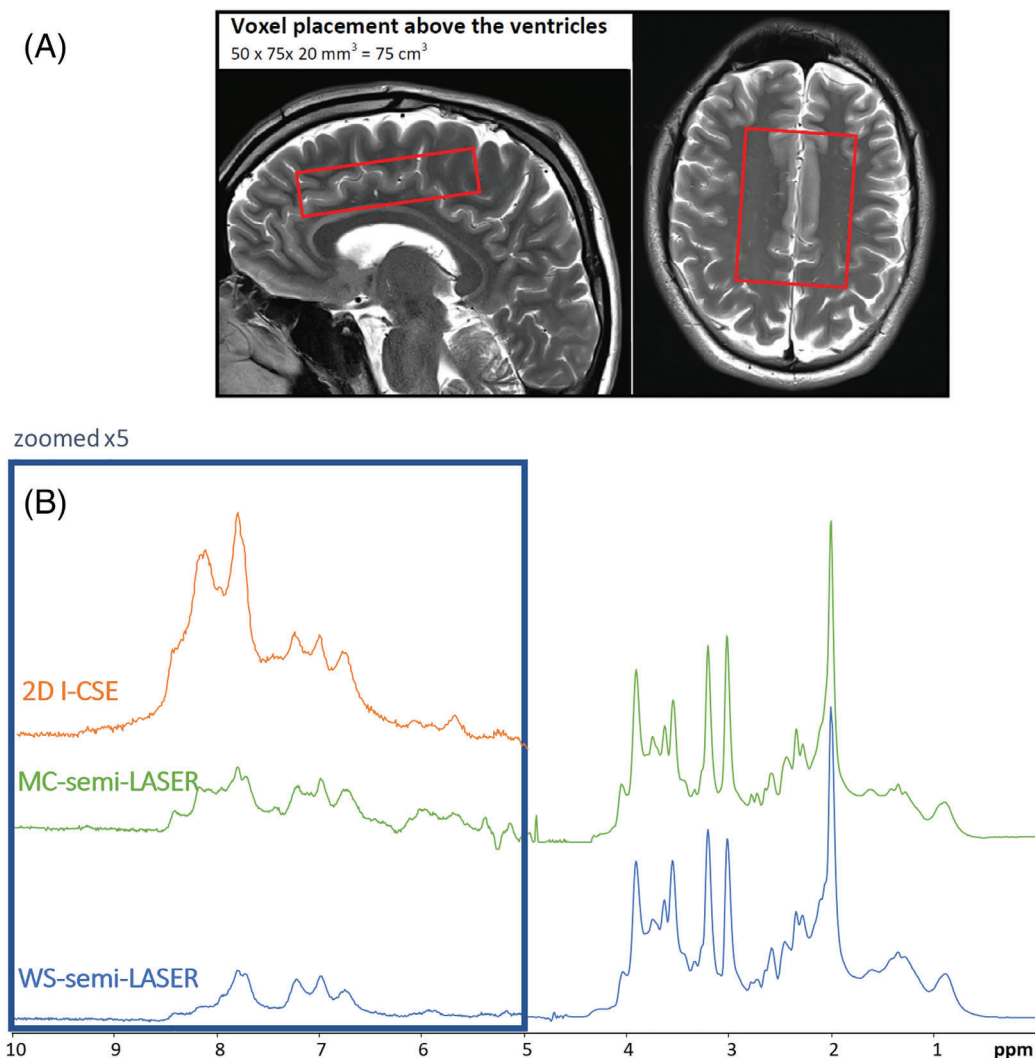The investigations were performed in compliance with the requirements by the Cantonal Ethics Board.

FIGURE 1 Illustration of VOI placement and spectral quality for a representative subject. **A)** The 75 cm³ VOI placed centrally above the lateral ventricles with 5 mm spacing. **B)** Full spectra (downfield and upfield parts) for the semi-LASER-based techniques and the downfield part for frequency-selective 2D I-CSE documenting the overall spectral quality for all three techniques. When comparing noise levels, the differences in total number of scans and differences in different water-scaling have to be kept in mind (number of acquisitions and total scan times: 640, 768, 1280 and 32, 32, 55 min for 2D I-CSE, MC-semi-LASER, and WS-semi-LASER, respectively. I-CSE and MC-semi-LASER scaled with the water signal from MC-semi-LASER, WS-semi-LASER scaled by a reference signal recorded with the same sequence, but without VAPOR. Identical length of the acquired FID, no apodization, downfield part scaled by a factor of 5 compared to the upfield spectra)

2.1.1 | WS-semi-LASER

A semi-LASER localization sequence[12] with hyperbolic secant adiabatic pulses (HS4, R = 20, duration 4 ms) was used with outer-volume suppression pulses in the direction of the non-adiabatic excitation pulse. The transmit voltage was optimized for maximum signal and VAPOR WS (135 Hz bandwidth, total duration of 765 ms) for minimal residual water for each subject. The TE and TR were 35 ms and 2500 ms, respectively. The transmit frequency was set to 7.3 ppm for WS spectra. With a bandwidth of 5 kHz for the adiabatic pulses, this corresponds to a shift in the VOI by +5% for the NAD$^+$ peak at 9.3 ppm and −11%

for the creatine peak at 3 ppm. To achieve very high SNR, 1280 averages were acquired in total, split into five recordings with 256 averages each (using a phase cycle of 16) and a total acquisition time of 55 min. Additionally, one fully relaxed single shot for a non-suppressed water spectrum was acquired for each recording with the transmit frequency on resonance at 4.7 ppm for referencing.

2.1.2 | MC-semi-LASER

The MC-semi-LASER sequence[16] used a MC pulse[17] of 22 ms and no OVS (TE/TR = 35/2500 ms, transmit

frequency = 7.3 ppm). The transmit voltage was optimized using the manufacturer's default B_1-mapping method. The 768 spectra were acquired in 24 recordings of 32 averages each (interleaved with the 2D I-CSE acquisition), which results in a total acquisition time of 32 min.

2.1.3 | 2D I-CSE

2D I-CSE[10] made use of 5 ms long (30 kHz bandwidth; 1 ms gradient ramps) gradient-modulated offset-independent adiabatic (GOIA)[18,19] pulses with WURST (16, 4) shape[20] for 2D ISIS localization (assisted by six OVS pulses for VOI prelocalization) and frequency-selective 90° excitation with a Gaussian-weighted sinc pulse (3 ms duration; 290 Hz bandwidth, center frequency at 9.8 ppm) followed by a 4.8 ms slice-selective refocusing Mao pulse (1250 Hz bandwidth). ISIS cycles were played out as in Ref. [10]. TE/TR was 10.2/3000 ms. The transmit voltage for the excitation pulse was derived using the manufacturer's default B_1-mapping method. As mentioned for MC-semi-LASER, scans were acquired in interleaved mode with 640 acquisitions in 32 min. Reference scans with the frequency-selective excitation on-resonance with water were also acquired.

In contrast to the original experiment design,[10] additional water-selective inversion pulses were added, where appropriate in the ISIS cycle,[21] to ensure positive longitudinal water magnetization after each of the ISIS steps.

An additional non-water-suppressed spectrum was acquired using a STEAM sequence (TE/TM/TR = 20/10/2500 ms) to determine relative weights and phases the signal combination of coil elements.

2.1.4 | Calibration scans

In single subjects, additional measurements were performed to quantify the NAD$^+$ signal and to get comparable data between the MRS sessions:

- For tissue segmentation and determination of gray matter (GM) and white matter (WM) contributions T_1-weighted images using MP-RAGE (TE/TR = 3/2500 ms, $1 \times 1 \times 1.1$ mm^3 resolution, 9° flip angle, non-selective inversion) were acquired.
- A TE series of non-WS spectra was used for distinction of CSF and parenchymal water.[22] Using the WS-semi-LASER sequence with VAPOR deactivated, eight scans with different TE were acquired (TE = 35, 1000, 50, 400, 200, 75, 100, 140 ms; TR = 6 s).

2.2 | Data processing

Data processing was performed using jMRUI[23] and Matlab (Math Works, Natick, MA; version R2019a).

2.2.1 | WS-semi-LASER

The 256 acquisitions in each of the five sets were frequency-aligned; then averaged and eddy-current-corrected with the corresponding water-reference signal. The residual water signal, which was usually smaller than the maximum metabolite signal, was removed using a Hankel Lanczos Singular Value Decomposition (HLSVD) filter. Finally, the five resulting spectra were frequency-aligned and averaged.

2.2.2 | MC-semi-LASER

Metabolite and water spectra were extracted in Matlab as described in Ref. [16]. This included eddy-current and frequency/phase correction, as well as optimized calculation of difference spectra. Subsequently, spectra from all series were frequency/phase aligned and averaged in jMRUI.

2.2.3 | 2D I-CSE

Coil combination based on the STEAM water-reference signals was performed in Matlab and is described in Supporting Information Data S1, which is available online. Eddy current correction, frequency alignment, and overall summation were done as described above. Residual water and upfield metabolite signals were removed using HLSVD filtering in jMRUI.

2.2.4 | Cohort average spectra

A cohort average spectrum with increased SNR was created for all three techniques using the raw spectra from each subject scaled by water reference data acquired for each case (see below in the quantitation section).

2.3 | Fitting procedure

Metabolite basis sets were simulated using VESPA[24] with timings according to the specific experimental settings. The simulation comprised digitized evolution under

the adiabatic pulses but neglected offset terms from slice-selection gradients. FiTAID[25] was used to fit the spectra and to calculate CRLB.

2.3.1 | MC- and WS-semi-LASER

The fit was performed in two major steps. First, the upfield part (fitting range: −1.2 to 4.2 ppm) was modeled, where 18 metabolites (aspartate; creatine [Cr]; ethanolamine; γ-aminobutyric-acid; glucose; glutamine; glutamate; glycine; glycerophosphorylcholine; glutathione; lactate; *myo*-inositol; *N*-acetylaspartate [NAA]; *N*-acetylaspartylglutamate; phosphocholine; phosphocreatine [PCr], phosphorylethanolamine; *scyllo*-inositol; taurine) and a macromolecular (MM) contribution were included. The MM spectrum was composed of 47 equally spaced Voigt lines (spacing: 0.08 ppm, range: 0.3–4.1 ppm, Lorentzian broadening: 15 Hz, Gaussian broadening: 5 Hz). The MM lines between 0 and 1.8 ppm were allowed to vary in phase to adapt to spurious lipid signal contributions. All upfield metabolite patterns were convolved in the fit model with a Voigt lineshape with equal Lorentzian and Gaussian broadening and identical phase and frequency offsets. A single Voigt line at 4.7 ppm (Lorentzian broadening of 8 Hz and Gaussian broadening of 5 Hz) was included to emulate a water signal for cases with imperfect HLSVD filtering of the residual water peak.

Second, the downfield part of the spectrum (fitting range: 5.8 to 9.8 ppm) was modeled with the upfield model kept fixed. The focus of this fit was on the spectral part with NAD$^+$ resonances between 8.7 and 9.4 ppm. The rest of the downfield spectrum (<8.7 ppm) was considered a background signal that was fitted with large model flexibility such that the baseline in the spectral region of interest was adequately described. Hence, <8.7 ppm, the spectrum was modeled by 68 equally spaced Voigt lines (spacing: 0.04 ppm; range: 5.9–8.6 ppm; Lorentzian broadening 8 Hz, common, but fitted Gaussian broadening). For NAD$^+$, the simulated spectral pattern for the H2, H4, and H6 protons (resonances between 8.7 and 9.4 ppm, spin system parameters from Ref. [5]) was used and convolved with a Voigt shape with a Gaussian width related to the other downfield signals and a fixed Lorentzian width, based on an assumed T_2 of 80 ms. All downfield resonances were modeled with the same phase.

CRLB for NAD$^+$ were calculated for the last step, that is, with a fitting range covering 5.8–9.8 ppm only and under the assumptions that the signal tail extending from the upfield spectrum represents the true background signal.

2.3.2 | 2D I-CSE

The fit model of the semi-LASER spectra was copied for I-CSE data but adapted in two aspects: (1) No upfield metabolites were included (frequency-selective excitation and residual signal eliminated with HLSVD). (2) Given the much larger amide signal in the case of I-CSE, the model was extended by one broad Voigt line representing the signal tail from amide resonances (line at 8.5 ppm, 50 Hz Lorentzian, and 105 Hz Gaussian broadening).

2.4 | Quantification

Differences in the VOI profiles for the 2D I-CSE and the semi-LASER methods were eliminated based on phantom measurements (assuming uniform metabolite distribution in vivo).

Conversion of the estimated peak area of NAD$^+$ to absolute concentration units was based on the fitted area of unsuppressed water from MC-semi-LASER (for MC-semi-LASER and 2D I-CSE) or from a unsuppressed and fully relaxed reference semi-LASER acquisition (for WS-semi-LASER) using Equation (3) in Ref. [26]. Reference measurements had not been acquired for all subjects but were taken from one typical case and applied to all. They included CSF correction and back-extrapolation to TE 0 for the water reference signal based on the multi-TE acquisitions and definition of the tissue content of the VOI in terms of WM and GM to define the water content to be used.

AMARES was used to fit all water reference spectra. The TE decay was analyzed using Excel's solver. WM and GM percentages of the VOI were determined from co-registered MP-RAGE data using a manual in-house segmentation tool. Water contents of 0.78 and 0.65 were used for GM and WM.[27] Moreover, to account for differences in effective VOI size between I-CSE and semi-LASER, the I-CSE data were scaled down by a factor 1.09 determined in a water phantom. The other numeric values as determined in one subject turned out to be: 11.4% CSF volume and a water T_2 of 69 ms from TE data; 39% and 61% of GM and WM brain tissue yielding an average water content of 70%. T_1 and T_2 corrections of the NAD$^+$ signal used an assumed T_1 of 800 ms for the case of semi-LASER and a T_2 of 80 ms for all techniques. Both values were deduced from Ref. [5], assuming T_2 to be longer and T_1 to be shorter at 3 T than at 11.7 T. For the nWE method, no T_1 correction was needed given that the native T_1 of NAD$^+$ is much shorter for that case.[5]

3 | RESULTS

Representative spectra for all three techniques from a single subject are presented in Figure 1B. Spectra from WS-semi-LASER and MC-semi-LASER cover the full spectral range (0–10 ppm), while the I-CSE spectrum is restricted to the downfield portion. They document the excellent spectral quality in terms of linewidth and SNR (the downfield part is scaled up by a factor of 5). They also illustrate obvious intensity differences in the downfield part-most likely due to effects of saturation/magnetization exchange, while differences in MC- and WS-semi-LASER in the upfield region are likely caused by differences in slice profiles and chemical shift displacement effects.

3.1 | Detection and identification of NAD+

Figure 2 shows cohort averaged downfield spectra from 10 subjects for all three techniques with a zoomed spectrum including the simulated spectral pattern of NAD+ to indicate the area that is relevant for NAD+ quantification. A singlet at 9.33 ppm is clearly detectable with all methods. It corresponds to the signal from the H2 proton of the nicotinamide moiety. The nWS methods show also signal contributions from H6 and H4. Both doublets clearly correspond to the expected signal from the simulated spectrum in the case of MC-semi-LASER, where those signals are stronger than in WS-semi-LASER and not confounded by the rising edge of the large signal from amide protons observed with the nWE technique. The fourth nicotinamide proton (H5) features a more complex spectral pattern and cannot be detected, while two singlet resonances from the adenine unit (H2 and H8) do correspond to small peaks in the MC-semi-LASER spectrum but cannot be assigned unambiguously, in particular as other metabolites contribute in this region.

3.2 | Quantification of NAD+

Figure 3 gives an example for the overall fit covering up- and downfield regions for a single subject and WS-semi-LASER as well as MC-semi-LASER, where up- and downfield spectra are present with opposed phase. Since the upfield fit is not evaluated by itself, an exact match was not essential.

Figure 4 illustrates model fitting of the downfield range, in particular for the targeted H4, H6, and H2 signals for all three techniques and a single subject case on the left and the cohort average on the right. Model fitting shows an acceptably good fit for all three techniques with the most convincing results for MC-semi-LASER. In the
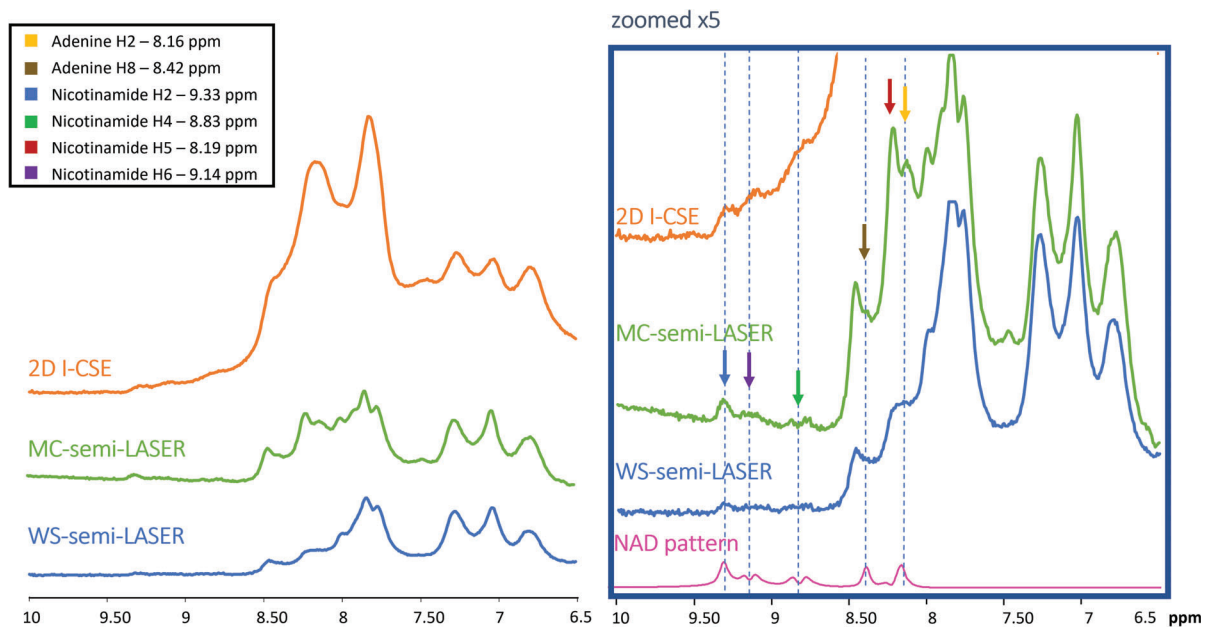

FIGURE 2 Averaged downfield cohort spectra from 10 subjects for all three methods, each plotted in the range between 6.5 and 10 ppm. The cohort averages were constructed after scaling by unsuppressed water to guarantee equal weight for each subject. Appropriate scaling (including the VOI size effect and compensation for the different water references) was also used to assure an akin scale between methods. Vertical scaling was increased fivefold for the right-hand side spectra to emphasize the NAD+ signal in comparison to the simulated NAD+ pattern (NAD+ peaks at 8.2 and 8.4 ppm removed from base spectra to minimize interference in modeling with large overlapping signals). Dashed lines indicate the fitted NAD+ peaks
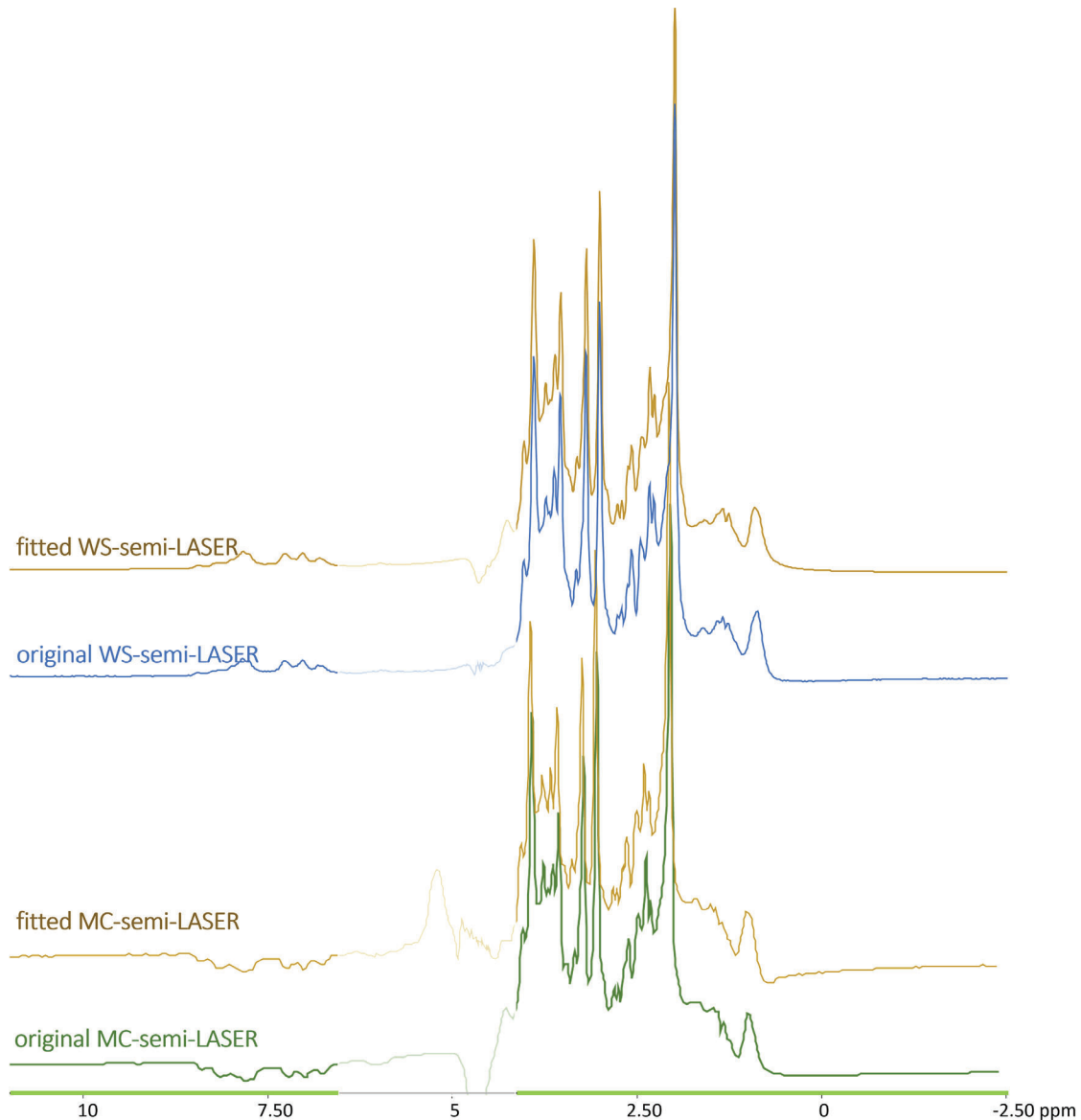
FIGURE 3 Illustration of model fitting for the semi-LASER techniques covering the full spectral range in a representative subject. The spectral range around the HLSVD filtered residual water was excluded from the fit. Using an additional resonance line to model the removed residual water allowed the correction of filtering effects leading to a baseline bias, which is even more prominent in the dispersion part of the spectrum

case of 2D I-CSE, the residues do not seem to contain noise only but also residual signal that was not captured well by the applied fit model, either because the tail of the amide signal was not well modeled or because small sideband signals are present originating from the water and upfield signals that were eliminated in postprocessing.

The resulting concentrations of NAD^+ obtained with the three techniques are given in Table 1 with and without relaxation corrections. Averaging the results from 10 subjects yielded relaxation-corrected estimated apparent NAD^+ concentrations of $54 \pm 25\,\mu M$ (WS-semi-LASER), $150 \pm 17\,\mu M$ (MC-semi-LASER), and $115 \pm 37\,\mu M$ (2D I-CSE), respectively (mean ± 1 cohort

SD). Somewhat more consistent values and very small fitting errors were obtained when fitting the cohort average spectrum: $58 \pm 5\,\mu M$ (WS-semi-LASER), $146 \pm 6\,\mu M$ (MC-semi-LASER), and $125 \pm 8\,\mu M$ (2D I-CSE), respectively (estimate ± 1 CRLB). The table also contains mean absolute CRLB for all three techniques with and without relaxation correction.

4 | DISCUSSION

Three MRS techniques with different approaches to deal with the water resonance have been evaluated for their
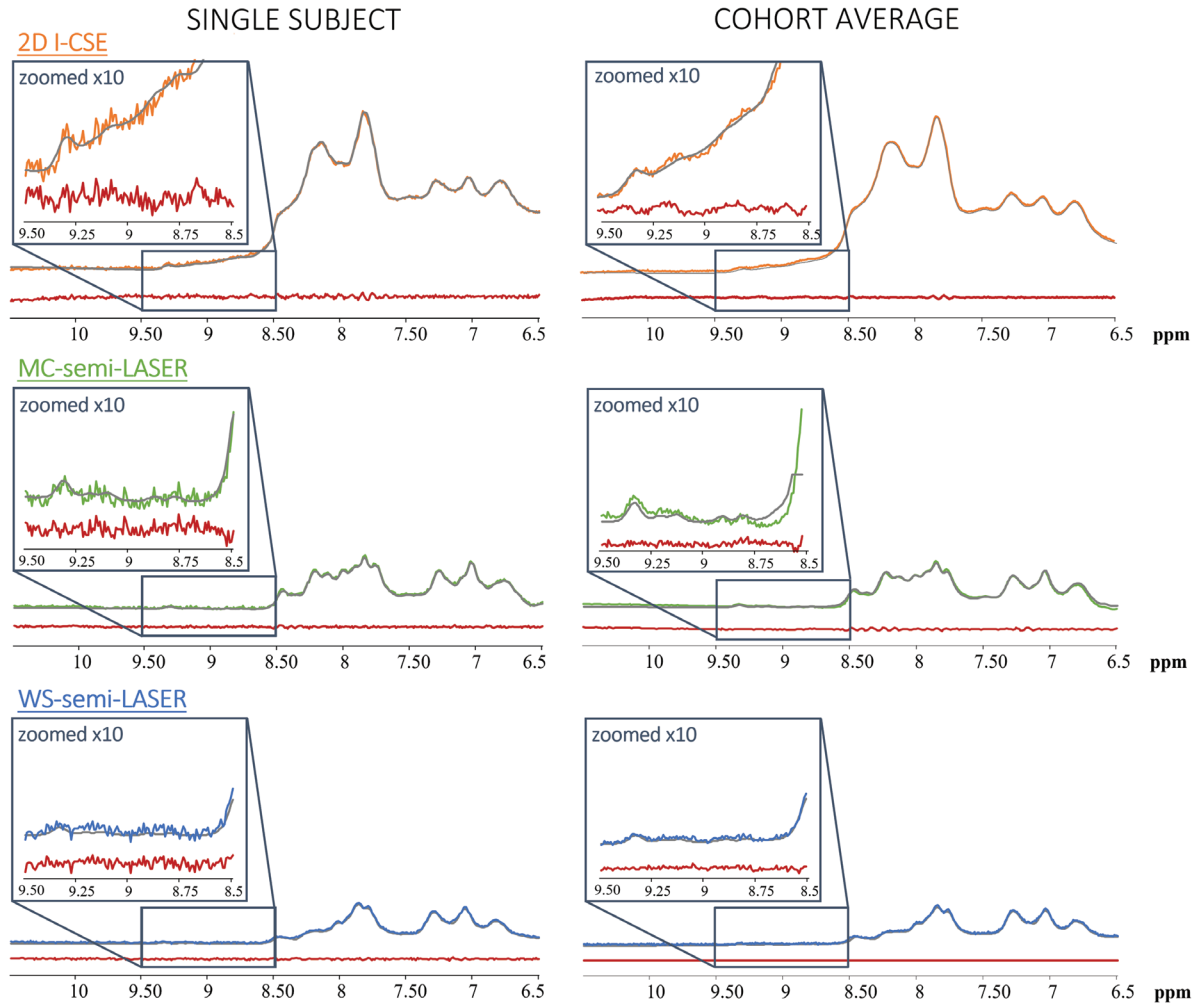
FIGURE 4 Illustration of the last step in model fitting for all three techniques where the parameters are optimized for the downfield part of the spectra only. Experimental (orange, green, and blue) and fitted (gray) spectra are overlaid, while residues (difference between experimental and fitted spectra in red) are plotted with an offset for clarity. Vertical scaling between methods as in Figure 2

TABLE 1 Quantitative results of tissue content estimation for NAD^+ [μM]

Technique	Cohort average spectrum				Individual spectra			
	Raw content	Raw CRLB	NAD^+ content	NAD^+ CRLB	Raw content	Raw CRLB	NAD^+ content	NAD^+ CRLB
WS-semi-LASER	36	3	58	5	33 ± 15	10 ± 4	54 ± 25	16 ± 7
MC-semi-LASER	90	4	146	6	93 ± 10	13 ± 2	150 ± 17	21 ± 3
2D I-CSE	108	7	125	8	99 ± 32	17 ± 3	115 ± 37	19 ± 3

Note: Estimated values in micromolar units for tissue content and CRLB are given for the cohort average spectrum on the left and corresponding averaged estimated values ± 1 SD from the results of individual spectra of the cohort are listed on the right. Results from all three techniques are provided without (left, labeled raw) and with T_1- and T_2-corrections for the NAD^+ signal.

potential to determine NAD^+ content in human brain at 3 T. This was combined with adapted prior knowledge fitting for quantification. Cohort data in terms of average estimated NAD^+ content, its variation over the cohort and fitting uncertainties for individual measurements have been obtained for 10 subjects each. The results indicate that using a high number of acquisitions, a large VOI and an optimized MR sequence enable in vivo detection and quantification of NAD^+ tissue content in human brain at 3 T. This may open the possibility for widespread use of NAD^+ as a further metabolic marker in non-invasive clinical MRS assays.

4.1 | Detection and quantification of NAD⁺

The downfield part of the cohort spectrum, which is depicted in Figure 2, allows a clear and unique identification of some of the NAD⁺ resonances in the range between 8.5 and 9.5 ppm with all three techniques. It is noteworthy that the H4 and H6 contributions are represented as resolved doublets at 3 T, which is not the case at higher fields[6,9] and adds trust in the assignment. The NAD⁺ responses between 6 and 8.5 ppm are overlapped by non-identified metabolite and/or MM resonances (with very strong amide resonances for the case of the nWE 2D I-CSE technique). In the zoomed cohort spectra in Figure 2 the peak at 9.33 ppm attributed to the H2 proton of NAD⁺ is clearly visible for all methods. In addition, both techniques without WS reveal distinct features from the contributions of the H6 and H4 NAD⁺ protons.

The raw NAD⁺ signal strength (reflected in the tissue content without relaxation correction) is largest for 2D I-CSE, followed by MC-semi-LASER. After T_2-correction, the estimated tissue content is highest for MC-semi-LASER, slightly lower for I-CSE, and considerably lower for WS-semi-LASER. This confirms the previously reported limited visibility of NAD⁺ signals in ¹H MRS, attributed to saturation transfer from water. The estimated tissue content of ∼144–150 μM indicates visibility of approximately 40% when referring to NAD⁺ brain tissue content determined by ³¹P-MRS (367 μM)[6] or invasive experiments on rat brain (355 μM).[5] The tissue concentration estimated in this work by MC-semi-LASER is virtually identical to what has been reported by Bagga et al.[9] but higher than the values reported by de Graaf et al.[6] for the human brain using ¹H-MRS techniques with similar experimental settings (i.e., without water excitation) but at a higher field strength. The reported values were 105 μM (30% visibility)[6] for a whole slice observed with an adiabatic double echo method (TE 18 ms) and about 145 μM (40% visibility)[9] in a 3D localized triple echo method (TE 19 ms; value for a mean age of 35 y and undoing a visibility factor mentioned for the calculation of the reported numbers). There is no obvious explanation for the lower result for the former study. The determined tissue content for NAD⁺ by I-CSE in our study is 15% lower than the value from MC-semi-LASER. This may partly be incidental given limited SNR and partly due to a bias in fitting caused by the amide resonance baseline. In addition, all these values are substantially lower than what had been reported by de Graaf et al. with a visibility of 66% for rat cortex at even higher field strength (slightly shorter TE [14 ms], visibility based on total creatine as reported in Ref. [5]).

4.2 | Fitting precision

Fitting precision for NAD⁺ as judged by CRLB was found to be quite good, given the partial overlap with background signals of an ill-defined nature. Mean CRLB of around 16 μM, corresponding to ∼30%, resulted for the single subject spectra from 1280 acquisitions in the WS case, while they were ∼21 μM (14%–17%) for the non-WS cases. The lower value for WS is explained by the lower noise with the 1.66 times more acquisitions in that case. Comparing MC with I-CSE, the raw fitting uncertainty is higher in the I-CSE spectra (larger overlap with background signals), but this is compensated by the smaller relaxation correction needed. Hence, the CRLB for all three methods as expressed in absolute terms after relaxation correction are equal if extrapolated to equal acquisition time. However, given the substantial underestimation of the NAD⁺ content with the WS method, relative precision is lowest for that case. Two factors may have helped to keep the CRLB fairly low. First, calculation of χ^2 in the frequency domain (although with a time domain signal model) allowed to restrict modeling to a well-defined downfield region of the whole spectrum preventing inaccuracies in the upfield modeling, which gives much bigger errors in absolute terms, to interfere with adapting to the tiny NAD⁺ signals. Second, modeling the main part of the downfield region with a flexible equally-spaced-line representation allowed to model neighboring signals with a high degree of freedom, such that not only the background, but also the overlapping parts of the NAD⁺ spectrum below 8.5 ppm could easily be adjusted to. Hence, the quantification of NAD⁺ in the current approach relied on the region between 8.7 and 9.4 ppm, where, for MC-semi-LASER, hardly any background signal is present, in particular since only the well-separated part of the NAD⁺ metabolite pattern was used for the analysis.

Given the somewhat arbitrary definition of the fit model and use of prior knowledge, the determined CRLB can only be taken as a very rough indicator for the precision of NAD⁺ tissue content estimation. A better indicator may be taken from the SD found over the cohort of healthy subjects. This includes robustness versus intersubject variation in the experimental setup. In this view, MC-semi-LASER clearly performs best with a coefficient of variance (CV) of 11% (similar to the CRLB, i.e., the lowest possible value) vs. 32% for I-CSE and 46% for WS-semi-LASER. Thus, with a cohort CV of ≤15%, MC-semi-LASER clearly performs well enough for clinical or clinical-research use.

To achieve such tight measurements, not only a large voxel size but also a large number of averages with a correspondingly long acquisition time of 32 min was needed.

Given that CRLB (and the cohort CV was of a similar size) scale inversely with the square root of the number of acquisitions, we expect that even with only half of the acquisition time, which is more realistic for patient investigations, a CV of $\leq 20\%$ can be obtained.

4.3 | Limitations

Fitting of the downfield part of the ^{1}H MR spectrum is challenging as the majority of the signals have not been fully identified, rendering straight linear-combination-model fitting with known base spectra impossible. Even for the well-assigned signals of the homo-carnosine resonances, stringent prior knowledge information is not available, since the exact resonance frequencies depend on pH. Hence, the model with equally spaced Voigt lines chosen to represent most of the downfield signals, although beneficial for NAD$^+$ quantification, does not allow for the evaluation of any other downfield metabolite signals.

Furthermore, to allow for adequate flexibility, but still also to limit the number of fitting parameters, some assumptions had to be taken to simplify and stabilize the fitting model. The T_2 of NAD$^+$ was assumed to be 80 ms, therefore, the Lorentzian linewidth was fixed and could not vary between the techniques. The assumed value of 80 ms was chosen based on the reported T_2 of 54 ms for 11.7 T[5] and the known trend for other metabolites for lower T_2s at ultrahigh field compared to 3 T.[28–30] Similarly, also the T_1 value for NAD$^+$ is not known for 3 T. Given the fairly long TR's used and the sub-second T_1 expected based on the findings at 11.7 T[5] and the known trend for longer T_1's at higher fields, no large effect for the concentration estimation is expected even if the assumed T_1 of 800 ms is not accurate.

Additional uncertainty for the accuracy of the absolute tissue content stems from the fact that we had not recorded the identical reference measurements for each subject and that the methods comparison is based on different measurement sessions and only partial overlap of subjects. However, we do not expect the CSF and GM/WM contributions in this very large VOI to vary very much between subjects or the correction factors for the use of different water reference acquisitions to carry much potential for significant differences between the results from the different methods.

A clear limitation of the current quantification is that the interpretation of the signal area fitted as NAD$^+$ pattern also crucially depends on the premise that no other metabolites give rise to major overlapping signal contributions at this end of the spectrum. If the approach is used to evaluate data from single patients, it will be crucial to make sure that no artifacts, like sidebands or ghost echoes, give rise to any spurious signal in this frequency range and that appearance of other metabolites should be considered in case of strongly altered NAD$^+$ concentration estimates.

The extent of the low MR-visibility of the WS-technique may have been exacerbated by the long duration of WS. Use of CHESS (selective RF pulses can be short) might restore some of the intensity.

4.4 | Perspectives

Hitherto, it has been assumed that detection of NAD$^+$ with ^{1}H MRS is only possible using ultrahigh field scanners and with specific localization sequences with frequency-selective excitation to leave the water magnetization undisturbed.[7,8,10] Here, we presented that the detection of NAD$^+$ is possible even at 3 T and in spite of water-presaturation with WS-semi-LASER, although with limited visibility and truly convincing only for the cohort average. However, replacing WS by MC with a limited period for saturation-exchange was shown to provide a well-suited detection technique yielding satisfactory results also for a single subject given relative CRLB of 14% and a cohort CV of 11%. Measuring NAD$^+$ with the same visibility as with nWE methods along with the full frequency range spectrum does not only make a better use of the required acquisition time, but also offers precise values for the commonly observed metabolite contents[11] at 3 T. In addition, MC has been implemented in multiple versions and is more widespread than the nWE techniques, which also seem more vulnerable in terms of additional unknown interfering signals and residual water and upfield signals.

In future studies, it will be of interest to investigate in more detail, what causes the signal reduction in WS compared to nWS examinations and what is the reason for the remaining limited visibility even with MC and nWE methods. In particular, it will be of interest whether the observed part of the total NAD$^+$ signal is from specifically compartmentalized (free?) NAD$^+$ while a major proportion of NAD$^+$ is invisible at these measurement conditions or if it is rather due to partial visibility of the whole pool of NAD$^+$. In addition, further shortening of TE when going from 2D I-CSE to 3D I-CSE with a technique that assures minimal periods of disequilibrium between NAD$^+$ and water magnetization and that assures that the water magnetization is left at $+B_0$ for all steps of the ISIS cycle[21] might render more of the NAD$^+$ signal visible. It will also be of interest to use MC-semi-LASER at higher fields to evaluate whether even shorter acquisition times are sufficient for NAD$^+$ quantification for even more realistic clinical scan times.

In terms of clinical applicability, obtaining only a proxy for real tissue content with parts of the compound invisible may be seen as a big hurdle, but it can also be considered as an opportunity since the "NAD^+-content" as determined with this method may also reflect relevant factors in the local environment of NAD^+ that might be of clinical or diagnostic relevance. To obtain a more extensive picture of NAD metabolism including the in vivo redox situation, ^{31}P MRS remains indispensable but comes with its own drawbacks of limited availability (ultrahigh field scanner, X-nuclear equipment) and methodologic challenges (unlocalized signal acquisition, differentiation of overlapping signals).

5 | CONCLUSIONS

Three techniques to access NAD^+ quantification in humans at 3 T-WS-semi-LASER, MC-semi-LASER, and 2D I-CSE, all used with an acquisition time > 30 min and targeting a large VOI, have been compared. NAD^+ was detected with severely limited visibility by WS-semi-LASER, whereas using non-water-suppression techniques-either based on MC or nWE-allowed its detection and quantification at a considerably higher visibility. Optimal acquisition conditions in terms of TE and the length of the period where magnetization transfer between water and the NAD^+ resonances may occur are achieved with the I-CSE technique. However, with this technique, signals of unspecific amide proton resonances in the range of 7.5–8.5 ppm become much stronger and at 3 T then yield an ill-defined background signal that interferes with robust and accurate quantification of the otherwise well isolated NAD^+ signals >8.5 ppm. MC, thus, proved to be the most precise and robust technique for clinical use of an NAD^+ assay, while the nWE technique is best suited to investigate amide signals with minimal effects of saturation transfer from water.

ORCID
Malgorzata Marjańska https://orcid.org/0000-0002-4727-2447
Edward John Auerbach https://orcid.org/0000-0003-4553-1545
Roland Kreis https://orcid.org/0000-0002-8618-6875

REFERENCES

1. Imai S, The NAD. The NAD World: a new systemic regulatory network for metabolism and aging--Sirt1, systemic NAD biosynthesis, and their importance. *Cell Biochem Biophys*. 2009;53:65-74.
2. Ying W. NAD+ and NADH in brain functions, brain diseases and brain aging. *Front Biosci*. 2007;12:1863-1888.
3. Lu M, Zhu XH, Zhang Y, Chen W. Intracellular redox state revealed by in vivo 31P MRS measurement of NAD+ and NADH contents in brains. *Magn Reson Med*. 2014;71:1959-1972.
4. Zhu XH, Lu M, Lee BY, Ugurbil K, Chen W. In vivo NAD assay reveals the intracellular NAD contents and redox state in healthy human brain and their age dependences. *Proc Natl Acad Sci U S A*. 2015;112:2876-2881.
5. de Graaf RA, Behar KL. Detection of cerebral NAD+ by in vivo 1H NMR spectroscopy. *NMR Biomed*. 2014;27:802-809.
6. de Graaf RA, De Feyter HM, Brown PB, Nixon TW, Rothman DL, Behar KL. Detection of cerebral NAD+ in humans at 7 T. *Magn Reson Med*. 2017;78:828-835.
7. Shemesh N, Dumez JN, Frydman L. Longitudinal relaxation enhancement in 1H NMR spectroscopy of tissue metabolites via spectrally selective excitation. *Chemistry*. 2013;19:13002-13008.
8. Goncalves SI, Ligneul C, Shemesh N. Short echo time relaxation-enhanced MR spectroscopy reveals broad downfield resonances. *Magn Reson Med*. 2019;82:1266-1277.
9. Bagga P, Hariharan H, Wilson NE, et al. Single-voxel 1H MR spectroscopy of cerebral nicotinamide adenine dinucleotide (NAD+) in humans at 7 T using a 32-channel volume coil. *Magn Reson Med*. 2020;83:806-814.
10. Dziadosz M, Bogner W, Kreis R. Non-water-excitation MR spectroscopy techniques to explore exchanging protons in human brain at 3 T. *Magn Reson Med*. 2020;84:2352-2363.
11. Hoefemann M, Adalid V, Kreis R. Optimizing acquisition and fitting conditions for 1H MR spectroscopy investigations in global brain pathology. *NMR Biomed*. 2019;32:e4161.
12. Marjanska M, Auerbach E. CMRR Spectroscopy Package https://www.cmrr.umn.edu/spectro/.
13. Scheenen TW, Klomp DW, Wijnen JP, Heerschap A. Short echo time 1H-MRSI of the human brain at 3 T with minimal chemical shift displacement errors using adiabatic refocusing pulses. *Magn Reson Med*. 2008;59:1-6.
14. Dreher W, Leibfritz D. New method for the simultaneous detection of metabolites and water in localized in vivo 1H nuclear magnetic resonance spectroscopy. *Magn Reson Med*. 2005;54:190-195.
15. Giapitzakis IA, Shao T, Avdievich N, Mekle R, Kreis R, Henning A. Metabolite-cycled STEAM and semi-LASER localization for MR spectroscopy of the human brain at 9.4 T. *Magn Reson Med*. 2018;79:1841-1850.
16. Döring A, Adalid V, Boesch C, Kreis R. Diffusion-weighted magnetic resonance spectroscopy boosted by simultaneously acquired water reference signals. *Magn Reson Med*. 2018;80:2326-2338.
17. Hwang TL, van Zijl PC, Garwood M. Asymmetric adiabatic pulses for NH selection. *J Magn Reson*. 1999;138:173-177.
18. Bogner W, Chmelik M, Andronesi OC, Sorensen AG, Trattnig S, Gruber S. In vivo 31P spectroscopy by fully adiabatic extended image selected in vivo spectroscopy: a comparison between 3 T and 7 T. *Magn Reson Med*. 2011;66:923-930.

19. Tannus A, Garwood M. Adiabatic pulses. *NMR Biomed*. 1997;10:423-434.

20. Andronesi OC, Ramadan S, Ratai EM, Jennings D, Mountford CE, Sorensen AG. Spectroscopic imaging with improved gradient modulated constant adiabaticity pulses on high-field clinical scanners. *J Magn Reson*. 2010;203:283-293.

21. Dziadosz M, Bogner W, Kreis R. A non-water-excitation MRS sequence with zero-echo time to investigate exchangeable moieties in the human brain at 3 T. *Proceedings of the 28th Annual Meeting of ISMRM*; 2020:2864.

22. Kreis R, Ernst T, Ross BD. Absolute quantitation of water and metabolites in the human brain. II. Metabolite concentrations. *Journal Magnetic Resonance Series B*. 1993;102:9-19.

23. Stefan D, Di Cesare F, Andrasescu A, et al. Quantitation of magnetic resonance spectroscopy signals: The jMRUI software package. *Meas Sci Technol*. 2009;20:104035.

24. Soher BJSP, Todd D, Steinberg J, Young K. VeSPA: integrated applications for RF pulse design, spectral simulation and MRS data analysis. *Proceedings of the 19th Annual Meeting of ISMRM*. Canada; 2011:1410.

25. Adalid V, Doring A, Kyathanahally SP, Bolliger CS, Boesch C, Kreis R. Fitting interrelated datasets: metabolite diffusion and general lineshapes. *Magma*. 2017;30:429-448.

26. Near J, Harris AD, Juchem C, et al. Preprocessing, analysis and quantification in single-voxel magnetic resonance spectroscopy: experts' consensus recommendations. *NMR Biomed*. 2021;34:e4257.

27. Kreis R, Ernst T, Ross BD. Development of the human brain: in vivo quantification of metabolite and water content with proton magnetic resonance spectroscopy. *Magn Reson Med*. 1993;30:424-437.

28. Michaeli S, Garwood M, Zhu XH, et al. Proton T2 relaxation study of water, N-acetylaspartate, and creatine in human brain using Hahn and Carr-Purcell spin echoes at 4 T and 7 T. *Magn Reson Med*. 2002;47:629-633.

29. de Graaf RA, Brown PB, McIntyre S, Nixon TW, Behar KL, Rothman DL. High magnetic field water and metabolite proton T_1 and T_2 relaxation in rat brain in vivo. *Magn Reson Med*. 2006;56:386-394.

30. Lopez-Kolkovsky AL, Meriaux S, Boumezbeur F. Metabolite and macromolecule T_1 and T_2 relaxation times in the rat brain in vivo at 17.2T. *Magn Reson Med*. 2016;75:503-514.

SUPPORTING INFORMATION

Additional supporting information may be found in the online version of the article at the publisher's website.

Data S1 Describes details of the coil combination algorithm and details of the calibrations steps for quantification